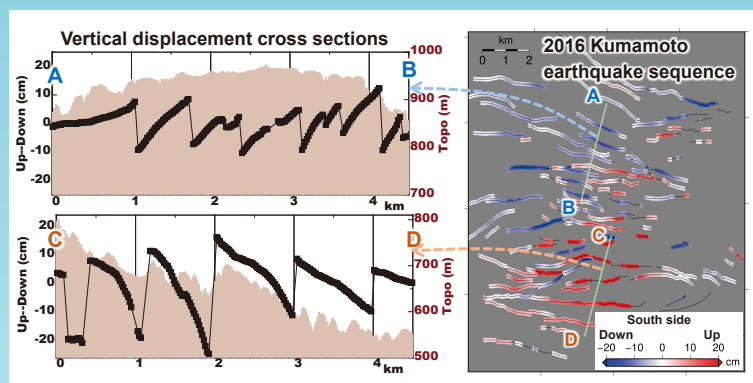


# Earth, Planets and Space

L-band Synthetic Aperture Radar: Current and future applications to Earth sciences



Society of Geomagnetism and Earth, Planetary and Space Sciences (SGEPSS)  
The Seismological Society of Japan  
The Volcanological Society of Japan  
The Geodetic Society of Japan  
The Japanese Society for Planetary Sciences



Springer Open

# Editorial Board (May 2022)

## **Editor-in-Chief**

Takeshi Sagiya, Nagoya University, Japan

## **Vice Editors-in-Chief**

Masahito Nosé, Nagoya University, Japan

Aitaro Kato, University of Tokyo, Japan

## **Editors**

Koki Aizawa

Hideo Aochi

Pascal Audet

Kiyoshi Baba

Joseph B.H. Baker

Nanan Balan

Stephan Christoph Buchert

Sonia Calvari

Xiaowei Chen

Peter Chi

Harold C. Connolly Jr

Phil Cummins

Hao Dong

Guangyu Fu

Hidenori Genda

Aditya Gusman

Tomasz Hadaś

Stuart Henrys

James Hickey

Hauke Hussmann

Mie Ichihara

Hidekatsu Jin

Art Jolly

Shunichi Kamata

Nobuki Kame

Katsuya Kaneko

Ikuo Katayama

Yoko Kebukawa

Kunihiro Keika

Kostas Konstantinou

Alexey Kuvshinov

Juanjo Ledo

Koji Matsuo

Yasunobu Miyoshi

Atsuko Namiki

Yasuhito Narita

Kazunari Nawa

Kiwamu Nishida

Hiroyo Ohya

Duggirala Pallamraju

Severine Rosat

Akinori Saito

Tatsuhiko Saito

David Shelly

Hisayoshi Shimizu

Wataru Suzuki

Youichiro Takada

Sunny Tam

Naoki Uchida

Yanbin Wang

Yih-Min Wu

Chuang Xuan

Takahiro Yamamoto

Yuhji Yamamoto

Tadashi Yamasaki

Yusuke Yokota

Yohei Yukutake

Seiji Zenitani

## **Advisory Board**

Benjamin Fong Chao

Bernard Chouet

Yoshimori Honkura

Toshihiko Iyemori

Hiroo Kanamori

Jun'ichiro Kawaguchi

Takafumi Matsui

Hitoshi Mizutani

Yasuo Ogawa

Toshitaka Tsuda

Zhongliang Wu

Kiyoshi Yomogida

## Journal Scope

***Earth, Planets and Space (EPS)*** is the official journal of Society of Geomagnetism and Earth, Planetary and Space Sciences, The Seismological Society of Japan, The Volcanological Society of Japan, The Geodetic Society of Japan, and The Japanese Society for Planetary Sciences.

EPS is a peer-reviewed, open-access journal published under SpringerOpen. It is an international journal covering scientific articles in the entire field of earth and planetary sciences, particularly geomagnetism, aeronomy, space science, seismology, volcanology, geodesy, and planetary science. EPS also welcomes articles in new and interdisciplinary subjects, and technical reports on instrumentation and software.

The journal was launched in 1998 and has since published over 4000 articles. All of them are available for free on SpringerLink:

<https://link.springer.com/journal/40623/volumes-and-issues>

More information about the journal, its article collections, and the submission process is available on the journal homepage:

<https://earth-planets-space.springeropen.com>

Submit your next research article to Earth, Planets and Space via:

<https://www.editorialmanager.com/eps>

Yours sincerely,

Prof. Takeshi Sagiya

Editor-in-Chief, *Earth, Planets and Space*

[eic@earth-planets-space.org](mailto:eic@earth-planets-space.org)

## PREFACE

## Open Access



# L-band Synthetic Aperture Radar: Current and future applications to Earth sciences

Yosuke Aoki<sup>1\*</sup>, Masato Furuya<sup>2</sup>, Francesco De Zan<sup>3</sup>, Marie-Pierre Doin<sup>4</sup>, Michael Eineder<sup>3</sup>, Masato Ohki<sup>5</sup> and Tim J. Wright<sup>6</sup>

Synthetic Aperture Radar (SAR) has been around for more than 40 years. The first civilian-use SAR satellite was SeaSat, launched by National Aeronautics Space Administration (NASA) in 1978 to monitor Earth's oceans. In early 1990s, we realized that SAR Interferometry (InSAR) is a powerful tool in delineating Earth's topography and deformation (e.g., Massonnet et al. 1993) because SAR can image broad areas with a high spatial resolution on the order of 10 m or less without a requirement of ground-based instruments. The advantage of SAR as a powerful imaging tool is also because it works day and night regardless of clouds.

SAR images taken from L-band satellites complement satellites at shorter wavelengths such as C- and X-bands. L-band SAR has lower resolution than C- and X-band images but are more coherent over time, especially in vegetated regions. L-band SAR data are typically easier to unwrap because of higher coherence and fewer fringes, but more susceptible to ionospheric effects.

L-band SAR satellites for InSAR include JERS-1 (1992–1998), ALOS (2006–2011), ALOS-2 (2014–present), and SAOCOM-1 (2017–present), which have a recurrence time of order a few weeks. Such recurrence times do not allow monitoring with high temporal resolution. However, after the launch of ALOS-4, NISAR, and Tandem-L in the next few years, we will be able to monitor Earth's surface every few days with L-band SAR. Therefore, the time is ripe to review what we have learned from previous and ongoing L-band missions, either spaceborne

or airborne and what we expect to learn from future missions.

This special issue consists of 11 papers on various topics, including earthquake and volcano deformation, land subsidence, landslide, and permafrost.

SAR images revealed that an earthquake rupture is almost always more complicated than a shear failure on a planar fault. SAR images have demonstrated that an earthquake rupture accompanies off-fault cracks and lineaments. Fujiwara et al. (2020) reviewed the observations of such secondary features associated with several onshore earthquakes in the last 25 years. The geometry of the faults on which triggered shallow slip occurs is variable; some faults are parallel to the main fault, and some are oblique or perpendicular to the main fault. However, they found some common features that tend to occur on pre-existing weakness. Therefore, a large earthquake in the future would also trigger shallow slips at the same location.

Hashimoto (2020) and Ishitsuka et al. (2020) investigated the 2016 Kumamoto earthquake ( $M_w=7.0$ ). Hashimoto (2020) investigated the first two years of post-seismic deformation from ALOS-2 images. He noticed that the L-band SAR images are coherent even if image pairs are separated for 2 years. He also noticed that some images are susceptible to ionospheric perturbations. The observed deformation field is complex; the time constant of displacement decay varies between 30 to 600 days in different locations, indicating that the observed deformation results from multiple origins. Afterslip with a mixed right-lateral normal faulting mechanism explains much of the observed deformation field, but the afterslip cannot explain observed deformation in some areas (Table 1).

\*Correspondence: yaoki@eri.u-tokyo.ac.jp

<sup>1</sup> Earthquake Research Institute, The University of Tokyo, Tokyo, Japan  
Full list of author information is available at the end of the article

**Table 1** List of SAR missions

Satellite	Band	Agency	Period
Seasat	L	US DoD	1978
ERS-1	C	ESA	1992–1996
JERS-1	L	JAXA	1992–1998
RADARSAT-1	C	CSA	1995–2013
ERS-2	C	ESA	1996–2011
SRTM	C, X	NASA	2000
ENVISAT	C	ESA	2002–2011
ALOS	L	JAXA	2006–2011
RADARSAT-2	C	CSA	2007–present
TerraSAR-X	X	DLR	2007–present
COSMO-SkyMed	X	ASI	2007–present
TanDEM-X	X	DLR	2010–present
ALOS-2	L	JAXA	2014–present
Sentinel-1	C	ESA	2014–present
SAOCOM	L	CONAE/ASI	2017–present
NISAR	L	NASA/ISRO	2021 (planned)
ALOS-4	L	JAXA	2022 (planned)
Tandem-L	L	DLR	(planned)

Ishitsuka et al. (2020) also investigated the postseismic deformation of the Kumamoto earthquakes, as Hashimoto (2020) did. They processed Sentinel-1 and ALOS-2 images to gain temporal resolution and detected deformation associated with groundwater movement. They interpreted postseismic subsidence which correlates with postseismic groundwater drawdown. They also detected seasonal deformation, which correlates with the seasonal variation of water level. The amplitude of seasonal deformation increased after the Kumamoto earthquake. These findings suggest that the Kumamoto earthquake changed aquifer permeability, compressibility, or both, leading to enhanced deformation associated with groundwater movement.

Fukushima et al. (2019) investigated another onshore earthquake, the 2017 Ormoc ( $M_w=6.5$ ), on the creeping Philippine fault in Leyte island, the Philippines. They processed ALOS and ALOS-2 images to find that the Philippine fault is creeping with a rate of  $33 \pm 11$  mm/year in the northern and central part of the Leyte island except for the locked portion where the Ormoc earthquake took place. An investigation of teleseismic records of the 1947 earthquake ( $M_s=6.9$ ) revealed that the Ormoc earthquake and the 1947 earthquake exhibit the repeating rupture within the same locked patch. They also inferred that the 1947 earthquake of  $M_s=6.9$  is nearly the maximum earthquake the Philippine fault can generate in the northern and central Leyte island. Their study demonstrates the utility of SAR images to assess large earthquakes along creeping faults.

InSAR is a powerful tool to investigate moderate-sized ( $M < 6.5$ ) earthquakes when local and regional seismic data are not available. Ghayournajarkar and Fukushima (2020) demonstrated another example with the 2017 Sefid Sang, northern Iran, earthquake ( $M_w=6.1$ ) from ALOS-2 and Sentinel-1 images. The observed displacement field fits well with both northeast- and southwest-dipping faults, but the aftershock distribution and orientation of active faults led them to conclude that the northeast-dipping fault is more favorable than the southwest-dipping fault. Their study demonstrates the utility of SAR images to investigate middle-sized earthquakes. Simultaneously, it demonstrates the difficulty in constraining which of two conjugate planes is responsible for the earthquake even with interferograms from both ascending and descending images.

Wang et al. (2019) and Narita et al. (2020) investigated volcano deformation. Wang et al. (2019) measured surface deformation near the vent of Asama Volcano, Japan, during its relatively dormant period (2014–2018). They employed not only ALOS-2 but also Sentinel-1 images to take advantage of more frequent acquisitions. Their time series analysis revealed surface deformation of up to 7 mm/year to the northeast and southeast of the summit. The surface deformation to the southeast of the summit is likely due to flank sliding, while the origin of that to the northeast of the summit is ambiguous. Although the area coincides with the lava deposit by a previous large eruption, thermal contraction is not responsible for this observed deformation because a theoretical consideration indicates the observed thermal contraction there should be negligible by now. The origin of the deformation there is either by flank sliding or due to hydrothermal activity. Flank sliding to the northeast of the summit should be northward, but the insensitivity to north–south displacements of spaceborne InSAR prevents the authors from confirming that the observed displacements there are due to flank sliding.

Narita et al. (2020) measured surface deformation between 2014 and 2018 from ALOS-2 and airborne PiSAR-L2 images. Utilizing airborne SAR images takes advantage of delineating arbitrary components of displacements, while interferograms from spaceborne SAR images are insensitive to north–south displacements because of the polar orbit of the satellite. The observed three-dimensional displacement field and its temporal evolution led Narita et al. (2020) to postulate two hydrothermal reservoirs at  $\sim 150$  and  $\sim 700$  m below sea level, with an impermeable bed between them. They interpreted that accelerating flux of hydrothermal fluid from depth to the deeper reservoir led to accelerating flux of hydrothermal fluid from the deeper to shallower reservoir. They concluded that the pressurization of

the shallower reservoir triggered a phreatic eruption in April 2018.

Various origins, including earthquake shaking and heavy rainfall, trigger landslides. SAR is a useful tool to detect and monitor landslides because of its high spatial resolution. Takada and Motono (2020) investigated details of a large landslide site at Mt. Onnebetsu-dake, northeastern Japan, in the last ~25 years from JERS-1, ALOS, and ALOS-2 images. The landslide velocity changes over time with a maximum of 60 mm/year of eastward velocity and ~20 mm/year of subsidence between 2014 and 2017. They interpreted that this velocity increase is due to increased pore pressure resulting from elevated annual rainfall during that period. They also found a shorter-term increase of landslide velocity in August 2016, by heavy rainfall. These observations indicate that both long- and short-term variations of rainfall affect the dynamics of landslides. The internal deformation within the landslide site indicates that the gravitational forces primarily drive the landslide.

While Takada and Motono (2020) focused on the dynamics of landslides, Ohki et al. (2020) focused on detecting landslides. They combined SAR polarimetry (PolSAR), InSAR, and Digital Elevation Model (DEM), to develop an algorithm to detect landslides. They applied their method to landslides by the 2017 heavy rainfall in northern Kyushu, Japan, and the 2018 Hokkaido Eastern Iburi, Japan, earthquake to find that polarimetric parameters, e.g., the alpha angle and Pauli components, are good indicators to discriminate damaged areas. They also found that supervised classification with PolSAR, InSAR, and DEM works well, although the classification accuracy depends on the training data's geological characteristics. These findings demonstrate the utility of SAR images to detect landslides quickly.

Recent global warming causes ground deformation due to excess melting of ground ice, and the processes to form subsequent terrain are called thermokarst. Abe et al. (2020) mapped subsidence due to thermokarst in Central Yakutia, Russia, with ALOS and ALOS-2 images. They detected a subsidence of 5–30 mm/year with seasonal variation in deforested areas, while the deformation in forested regions is negligible. This difference is consistent with the thermokarst dynamics through freezing and thawing. Also, the observation from the SAR images is consistent with field measurements and optical images. They found that L-band SAR images are useful in long-term monitoring permafrost areas because of persistent coherence.

Land subsidence of natural and anthropogenic origin, as well as global warming, is an issue that threatens human life. Herrera-García et al. (2021) recently reported

that land subsidence would pose 635 million people at risk by 2040. SAR is a powerful tool to detect and monitor land subsidence because of its high spatial resolution. Li et al. (2020) found from ALOS images that more than 122 km<sup>2</sup> of the Pearl River Delta, southern China, subsided by more than 30 mm/year between 2006 and 2011. In particular, the front part of the delta and the coastal area were subsiding by more than 50 mm/year. These observations led Li et al. (2020) to interpret that the subsidence is partly due to the thick, soft soil layer and partly due to human interference, such as reclamation, groundwater extraction, and urban construction.

This special issue demonstrates the utility of SAR images, L-band SAR images in particular, for various Earth Science applications including, but not limited to, earthquake and volcano deformation, landslide, glaciology, and land subsidence. In the next few years, the launch of new L-band satellites, including ALOS-4, NISAR, and Tandem-L, will give us a powerful new tool with which to make exciting discoveries, in particular by combining these L-band images with pre-existing C- and X-band SAR images.

#### Abbreviations

ALOS: Advanced Land Observing Satellite; ASI: Agenzia Spaziale Italiana (Italian Space Agency); CONAE: Comisión Nacional de Actividades Espaciales (National Space Activities Commission of Argentina); COSMO-SkyMed: Constellation of Small Satellites or Mediterraneanbasin Observation; CSA: Canadian Space Agency; DLR: Deutsches Zentrum für Luft- und Raumfahrt (German Aerospace Center); ENVISAT: Environmental Satellite; ERS: European Remote-Sensing Satellite; ESA: European Space Agency; InSAR: Synthetic Aperture Radar Interferometry; ISRO: Indian Space Research Organization; JAXA: Japan Aerospace Exploration Agency; NASA: National Aeronautics Space Administration; SAR: Synthetic Aperture Radar; TanDEM-X: TerraSAR add-on for Digital Elevation Measurement; US DoD: United States Department of Defense.

#### Acknowledgements

We thank authors and reviewers who contributed to organize this special issue. We also thank Editor-in-Chief Yasuo Ogawa for recommending to organize this special issue.

#### Authors' contribution

All authors served as guest editors for this special issue, YA being the lead guest editor. All authors read and approved the final manuscript.

#### Ethical approval and consent to participate

Not applicable.

#### Consent for publication

Not applicable.

#### Competing interests

The authors declare that they have no competing interests.

#### Author details

<sup>1</sup> Earthquake Research Institute, The University of Tokyo, Tokyo, Japan.

<sup>2</sup> Department of Natural History Science, Hokkaido University, Sapporo, Japan.

<sup>3</sup> Remote Sensing Technology Department, German Aerospace Center, Weßling, Germany.

<sup>4</sup> Institut Des Sciences de La Terre, Université Grenoble Alpes, Grenoble, France.

<sup>5</sup> Japan Aerospace Exploration Agency, Chofu, Japan.

<sup>6</sup> COMET, School of Earth and Environment, University of Leeds, Leeds, UK.

Received: 15 January 2021 Accepted: 15 January 2021

Published online: 23 February 2021

**References**

- Abe T, Iwahana G, Efremov PV, Desyatkin AR, Kawamura T, Fedorov A, Zhegusov Y, Yanagiya K, Tadono T (2020) Surface displacement revealed by L-band InSAR analysis in the Mayya area, Central Yakutia, underlain by continuous permafrost. *Earth Planets Space* 72:138. <https://doi.org/10.1186/s40623-020-01266-3>
- Fukushima Y, Hashimoto M, Miyazawa M, Uchida N, Taira T (2019) Surface creep rate distribution along the Philippine fault, Leyte Island, and possible repeating of Mw~6.5 earthquakes on an isolated locked patch. *Earth Planets Space* 71:118. <https://doi.org/10.1186/s40623-019-1096-5>
- Fujiwara S, Nakano T, Morishita Y (2020) Detection of triggered shallow slips caused by large earthquakes using L-band SAR interferometry. *Earth Planets Space* 72:119. <https://doi.org/10.1186/s40623-020-01239-6>
- Ghayournajarkar N, Fukushima Y (2020) Determination of the dipping direction of a blind reverse fault from InSAR: case study on the 2017 Sefid Sang earthquake, northeastern Iran. *Earth Planets Space* 72:64. <https://doi.org/10.1186/s40623-020-01190-6>
- Hashimoto M (2020) Postseismic deformation following the 2016 Kumamoto earthquake detected by ALOS-2/PALSAR-2. *Earth Planets Space* 72:154. <https://doi.org/10.1186/s40623-020-01285-0>
- Herrera-García G, Ezquerro P, Tomás R, Béjar-Pizarro M, López-Vinielles J, Rossi M, Mateos RM, Carreón-Freyre D, Lambert J, Teatini P, Cabrai-Cano E, Erkens G, Galloway D, Hung W-C, Kakar N, Sneed M, Tosi L, Wang H, Ye S (2021) Mapping the global threat of land subsidence. *Science* 371:34–36. <https://doi.org/10.1126/science.abb8549>
- Ishitsuka K, Tsuji T, Lin W, Kagabu M, Shimada J (2020) Seasonal and transient surface displacements in the Kumamoto area, Japan, associated with the 2016 Kumamoto earthquake: implications for seismic-induced groundwater level change. *Earth Planets Space* 72:144. <https://doi.org/10.1186/s40623-020-01275-2>
- Li G, Feng G, Xiong Z, Liu Q, Xie R, Zhu X, Luo S, Du Y (2020) Surface deformation evolution in the Pearl River Delta between 2006 and 2011 derived from the ALOS1/PALSAR images. *Earth Planets Space* 72:179. <https://doi.org/10.1186/s40623-020-01310-2>
- Massoneet D, Rossi M, Camona C, Adragna F, Peltzer G, Feigl K, Rabaute T (1993) The displacement field of the Landers earthquake mapped by radar interferometry. *Nature* 364:138–142. <https://doi.org/10.1038/364138a0>
- Narita S, Ozawa T, Aoki Y, Shimada M, Furuya M, Takada Y, Murakami M (2020) Precursory ground deformation of the 2018 phreatic eruption on Iwo-Yama volcano, revealed by four-dimensional joint analysis of airborne and spaceborne InSAR. *Earth Planets Space* 72:145. <https://doi.org/10.1186/s40623-020-01280-5>
- Ohki M, Abe T, Tadono T, Shimada M (2020) Landslide detection in mountainous forest areas using polarimetry and interferometric coherence. *Earth Planets Space* 72:67. <https://doi.org/10.1186/s40623-020-01191-5>
- Takada Y, Motono G (2020) Spatiotemporal behavior of a large-scale landslide of Mt Onnebetsu-dake, Japan, detected by three L-band SAR satellites. *Earth Planets Space* 72:1331. <https://doi.org/10.1186/s40623-020-01265-4>
- Wang X, Aoki Y, Chen J (2019) Surface deformation of Asama Volcano, Japan, detected by time series InSAR combining persistent distributed scatterers, 2014–2018. *Earth Planets Space* 71:121. <https://doi.org/10.1186/s40623-019-1104-9>

**Publisher's Note**

Springer Nature remains neutral with regard to jurisdictional claims in published maps and institutional affiliations.

# Detection of triggered shallow slips caused by large earthquakes using L-band SAR interferometry

Satoshi Fujiwara\*, Takayuki Nakano and Yu Morishita

*Earth, Planets and Space* 2020, 72:119 DOI: 10.1186/s40623-020-01239-6

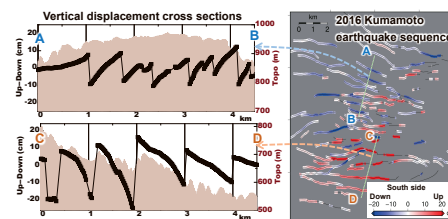
Received: 14 February 2020, Accepted: 22 July 2020, Published: 13 August 2020



## Abstract

Interferograms pertaining to large earthquakes typically reveal the occurrence of elastic deformations caused by the earthquake along with several complex surface displacements. In this study, we identified displacement lineaments from interferograms; some of which occur on the shallow section of seismogenic faults. However, such displacements are typically located away from the hypocenter, and they are considered as triggered shallow slips. We found that the triggered shallow slips had a varied nature, as follows. (1) No evidence has yet been obtained regarding the generation of large seismic motion via triggered shallow slips; thus, their occurrence is seldom considered a cause of major earthquakes. However, we found that a movement of triggered shallow slip associated with an  $M_6$ -class earthquake occurred on an active fault that has previously caused an  $M_7$ -class earthquake. (2) At certain locations, several parallel displacement lineaments have been discovered. During the Kumamoto earthquake sequence in 2016, the strain created by the main shock and the motion of triggered shallow slips coincided at a specific location, resulting in the creation of parallel triggered shallow slips by the main shock. Conversely, at another location, the movements of the main shock and triggered shallow slips did not match, since the main shock was simply a trigger, whereas the latter parallel triggered shallow slips are likely a means for releasing previously accumulated strain. (3) The fault scaling law—which states that the length and displacement of a fault are proportional—does not hold true for triggered shallow slips. However, the parallel triggered shallow slips show a relationship between horizontal spacing and its displacement. This may be attributed to immobility in deep locations. These results lead to the following conclusions. Large earthquakes tend to trigger shallow slips on the pre-existing faults. Subsequently, these triggered shallow slips release accumulated strain by causing fault motions, which in turn result in displacement lineaments. The occurrence of such passive faulting creates weak, mobile fault planes that repeatedly move at the same location. These triggered shallow slips cause the diversity among active faults as a result.

**Keywords:** L-band SAR interferometry, JERS-1, ALOS, ALOS-2, Earthquake, Displacement lineament, Triggered shallow slip



Graphical abstract

\*Corresponding author: Satoshi Fujiwara, fujiwara-s2vq@mlit.go.jp

# Surface creep rate distribution along the Philippine fault, Leyte Island, and possible repeating of $M_w \sim 6.5$ earthquakes on an isolated locked patch

Yo Fukushima\*, Manabu Hashimoto, Masatoshi Miyazawa, Naoki Uchida and Taka'aki Taira

*Earth, Planets and Space* 2019, 71:118 DOI: 10.1186/s40623-019-1096-5

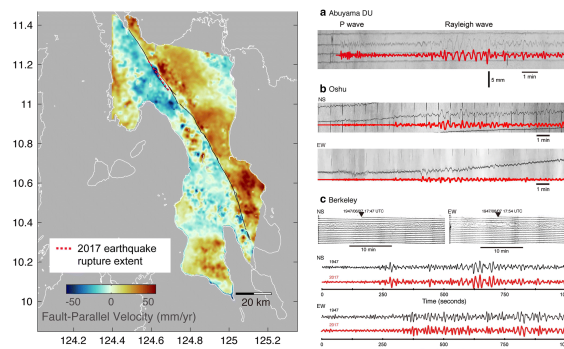
Received: 1 May 2019, Accepted: 23 October 2019, Published: 9 November 2019



## Abstract

Active faults commonly repeat cycles of sudden rupture and subsequent silence of hundreds to tens of thousands of years, but some parts of mature faults exhibit continuous creep accompanied by many small earthquakes. Discovery and detailed examination of creeping faults on land have been in a rapid progress with the advent of space-borne synthetic aperture radar interferometry. In this study, we measured the spatial variation of the creep rate along the Philippine fault on Leyte Island using ALOS/PALSAR data acquired between October 2006 and January 2011. Prominent creep of  $33 \pm 11$  mm/year was estimated in northern and central parts of the island except for a locked portion around latitude  $11.08$ – $11.20^\circ$ N. We compared the creep rate distribution along the fault with the slip distribution of the 2017  $M_w$  6.5 Ormoc earthquake which occurred in northern Leyte, estimated from the displacements mapped by ALOS-2/PALSAR-2 interferometric data. The estimated slip of the 2017 earthquake amounted up to 2.5 m and to moment magnitude of 6.49, with the dominant rupture area coinciding with the locked portion identified from the interseismic coupling analysis. Teleseismic waveforms of the 2017 earthquake and another event that occurred in 1947 ( $M_s$  6.9) exhibit close resemblance, indicating two ruptures of rather similar locations and magnitudes with a time interval of 70 years.

**Keywords:** Philippine fault, Leyte Island, Crustal deformation, SAR interferometry, InSAR, Fault creep, Repeating earthquake, Characteristic earthquake, Historical seismograms



Graphical abstract

\*Corresponding author: Yo Fukushima, fukushima@irides.tohoku.ac.jp

# Surface deformation of Asama volcano, Japan, detected by time series InSAR combining persistent and distributed scatterers, 2014–2018

Xiaowen Wang\*, Yosuke Aoki and Jie Chen

*Earth, Planets and Space* 2019, 71:121 DOI: 10.1186/s40623-019-1104-9

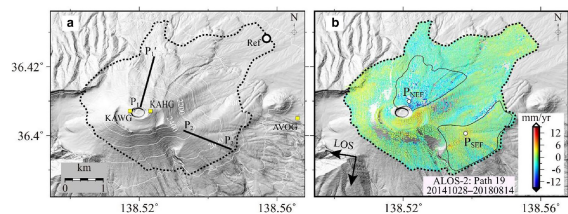
Received: 22 July 2019, Accepted: 1 November 2019, Published: 14 November 2019



## Abstract

Asama volcano is one of the most active volcanoes in Japan. Spatially dense surface deformation at Asama volcano has rarely been documented because of its high topography and snow cover around the summit. This study presents the first interferometric synthetic aperture radar (InSAR) observation of ground deformation at Asama volcano with 120 Sentinel-1 SAR images from both ascending and descending tracks and 20 descending ALOS-2 images acquired between 2014 and 2018. We exploited both persistent and distributed scatterers to overcome decorrelation of SAR signals and applied a three-dimensional unwrapping method to retrieve the displacement time series efficiently. Our observations reveal an asymmetric deformation around the volcano with two main deformation regions on the northeast and southeast flanks, respectively. The northeast flank (NEF) exhibits line-of-sight (LOS) extensions in all the three SAR datasets with maximum velocities of  $-14$ ,  $-10$ , and  $-12$  mm/year for the descending ALOS-2, ascending, and descending Sentinel-1 measurements, respectively. The southeast flank (SEF) shows LOS extensions in the ascending observations and LOS shortening in the descending observations with velocities between  $-12$  and  $9$  mm/year. Decomposition of the LOS displacements reveals nearly pure subsidence at the NEF, while the SEF exhibits a substantial eastward component as well as subsidence. Comparisons of the vertical subsidence at two continuous GNSS stations near the summit crater with our InSAR observations indicate small discrepancies smaller than  $4$  mm/year. We interpreted that the subsidence at the NEF of Asama is primarily due to the hydrothermal activity, while the deformation at SEF is plausibly due to flank instability. We highlight that efforts should be taken to monitor the slope instability at Asama volcano in the future.

**Keywords:** Asama volcano, InSAR, Volcano deformation, Persistent scatterers, Distributed scatterers, Slope instability



Graphical abstract

\*Corresponding author: Xiaowen Wang, insarwxw@gmail.com

# Determination of the dipping direction of a blind reverse fault from InSAR: case study on the 2017 Sefid Sang earthquake, northeastern Iran

Nematollah Ghayournajarkar\* and Yo Fukushima

*Earth, Planets and Space* 2020, 72:64 DOI: 10.1186/s40623-020-01190-6

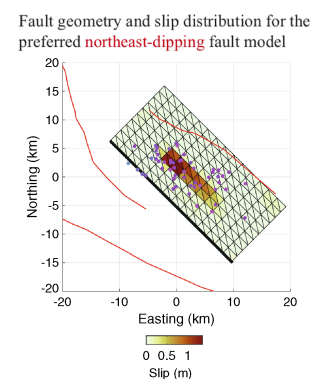
Received: 22 January 2020, Accepted: 28 April 2020, Published: 12 May 2020



## Abstract

Determining the fault parameters of an earthquake is fundamental for studying the earthquake physics, understanding the seismotectonics of the region, and forecasting future earthquake activities in the surrounding area. Dense crustal deformation data such as Interferometric Synthetic Aperture Radar (InSAR) are useful for fault parameter determination, but determining the dipping direction of a blind fault is often challenging when the size of the earthquake is not large ( $M < 7$ ) or when the coverage of the deformed area is limited to capture the details of rupture. The 5th April 2017, Mw 6.1 earthquake occurred near the city of Sefid Sang, northeast of Iran, provides an excellent case for exploring the potential of InSAR data for determining the dipping direction of a blind reverse fault. Using Advanced Land Observing Satellite-2 (ALOS-2) and Sentinel-1A interferograms of four different observation directions and a fault slip inversion method that allows thorough exploration of the fault geometry led to two candidates of reverse fault models, dipping either to the northeast or the south. The results show that the fault models of both dipping directions explain the data well, with a slight advantage in the northeast-dipping fault model in terms of the misfit when the atmospheric corrections were applied. The northeast-dipping fault model is, in addition, more consistent with the strike of the mapped active faults in the region and with the aftershock distribution, from which we infer that the 2017 Sefid Sang earthquake occurred on a northeast-dipping dextral-reverse fault. The preferred fault model has a strike angle of  $314.8^\circ$ , dip angle of  $47.4^\circ$  and rake angle of  $130.3^\circ$ , and a slip distribution of maximum  $1.35$  m at depth of  $5$  km equivalent to Mw 6.0. This study illuminates the difficulty of determining the dipping direction of blind faults even with InSAR measurements from multiple directions, but also that correcting for the atmospheric noise and comparing with other kinds of data can help infer the fault dipping direction.

**Keywords:** InSAR, Sefid Sang earthquake, Blind reverse fault, Coseismic deformation, Northeastern Iran, ALOS-2, Sentinel-1A



Graphical abstract

\*Corresponding author: Nematollah Ghayournajarkar, nghayour@dc.tohoku.ac.jp

# Landslide detection in mountainous forest areas using polarimetry and interferometric coherence

Masato Ohki\*, Takahiro Abe, Takeo Tadono and Masanobu Shimada

*Earth, Planets and Space* 2020, 72:67 DOI: 10.1186/s40623-020-01191-5

Received: 16 January 2020, Accepted: 4 May 2020, Published: 13 May 2020

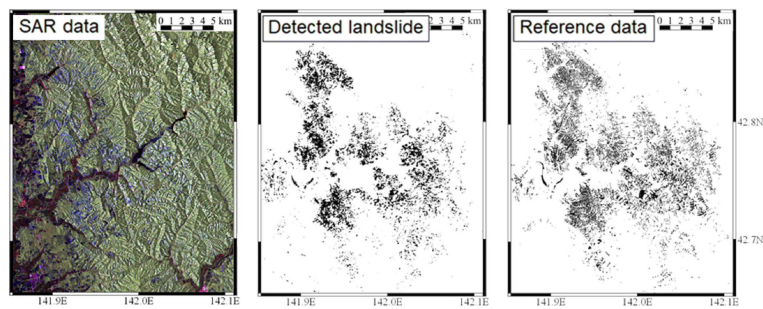


## Abstract

The cloud-free, wide-swath, day-and-night observation capability of synthetic aperture radar (SAR) has an important role in rapid landslide monitoring to reduce economic and human losses. Although interferometric SAR (InSAR) analysis is widely used to monitor landslides, it is difficult to use that for rapid landslide detection in mountainous forest areas because of significant decorrelation. We combined polarimetric SAR (PolSAR), InSAR, and digital elevation model (DEM) analysis to detect landslides induced by the July 2017 Heavy Rain in Northern Kyushu and by the 2018 Hokkaido Eastern Iburi Earthquake. This study uses fully polarimetric L-band SAR data from the ALOS-2 PALSAR-2 satellite. The simple thresholding of polarimetric parameters (alpha angle and Pauli components) was found to be effective. The study also found that supervised classification using PolSAR, InSAR, and DEM parameters provided high accuracy, although this method should be used carefully because its accuracy depends on the geological characteristics of the training data.

Regarding polarimetric configurations, at least dual-polarimetry (e.g., HH and HV) is required for landslide detection, and quad-polarimetry is recommended. These results demonstrate the feasibility of rapid landslide detection using L-band SAR images.

**Keywords:** Synthetic aperture radar (SAR), ALOS-2, Disaster monitoring, 2018 Hokkaido Eastern Iburi Earthquake, July 2017 Heavy Rain in Northern Kyushu, Machine learning



Graphical abstract

\*Corresponding author: Masato Ohki, ohki.masato@jaxa.jp

# Spatiotemporal behavior of a large-scale landslide at Mt. Onnebetsu-dake, Japan, detected by three L-band SAR satellites

Youichiro Takada\* and George Motono

*Earth, Planets and Space* 2020, 72:131 DOI: 10.1186/s40623-020-01265-4

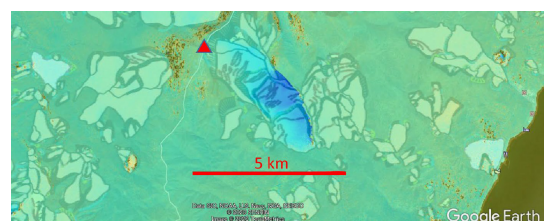
Received: 8 April 2020, Accepted: 2 September 2020, Published: 11 September 2020



## Abstract

We applied differential InSAR analysis to the Shiretoko Peninsula, northeastern Hokkaido, Japan. All the interferograms of long temporal baseline (~3 years) processed from SAR data of three L-band satellites (JERS-1, ALOS, ALOS-2) commonly indicate remarkable phase changes due to the landslide movement at the southeastern flank of Mt. Onnebetsu-dake, a Quaternary stratovolcano. The area of interferometric phase change matches to known landslide morphologies. Judging from the timing of the SAR image acquisitions, this landslide has been moving at least from 1993 to the present. Successive interferograms of 1-year temporal baseline indicate the temporal fluctuation of the landslide velocity. Especially for the descending interferograms, the positive line-of-sight (LOS) length change, which indicates large subsidence relative to the horizontal movement, is observed in the upslope section of the landslide during 1993–1998, while the negative LOS change is observed in the middle and the downslope section after 2007 indicating less subsidence. The landslide activity culminates from 2014 to 2017: the eastward and the vertical displacement rates reach ~6 and ~2 cm/yr, respectively. Utilizing high spatial resolution of ALOS and ALOS-2 data, we investigated velocity distribution inside the landslide. During 2007–2010, the eastward component of surface displacement increases toward the east, implying that the landslide extends toward the east. During 2014–2017, the vertical displacement profile exhibits spatially periodic uplift and subsidence consistent with surface gradient, which indicates the ongoing deformation driven by gravitational force. Heavy rainfall associated with three typhoons in August 2016 might have brought about an increase in the landslide velocity, possibly due to elevated pore-fluid pressure within and/or at the base of the landslide material. Also, annual rainfall would be an important factor that prescribes the landslide velocity averaged over 3 years.

**Keywords:** Slow-moving landslide, L-band, InSAR, JERS-1, ALOS, ALOS-2, Hokkaido



Graphical abstract

\*Corresponding author: Youichiro Takada, takaday@sci.hokudai.ac.jp

# Surface displacement revealed by L-band InSAR analysis in the Mayya area, Central Yakutia, underlain by continuous permafrost

Takahiro Abe\*, Go Iwahana, Petr V. Efremov, Alexey R. Desyatkin, Takumi Kawamura, Alexander Fedorov, Yuri Zhegusov, Kazuki Yanagiya and Takeo Tadono

*Earth, Planets and Space* 2020, 72:138 DOI: 10.1186/s40623-020-01266-3

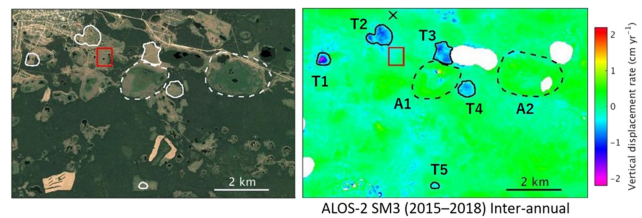
Received: 22 March 2020, Accepted: 4 September 2020, Published: 22 September 2020



## Abstract

Recent increases in global temperature have stimulated permafrost degradation associated with landform deformation caused by the melting of excess ground ice (thermokarst). Central Yakutia is underlain by ice-rich continuous permafrost, and there are complicated permafrost-related features in forested and deforested areas. This situation makes thermokarst monitoring necessary over a wide area to achieve a better understanding of its dynamics. As a case study, we applied L-band InSAR analysis to map surface subsidence due to thermokarst in this area and to demonstrate the suitability of L-band SAR for such monitoring. Our results show that InSAR detected subsidence/uplift signals in deforested areas and alasses; whereas, there were few ground deformation signals in forested areas with middle coherence. The InSAR stacking process, including both seasonal and inter-annual displacements, showed subsidence in deforested areas during 2007–2010 and 2015–2018, in the range of 0.5–3 cm yr<sup>-1</sup>. We also estimated the inter-annual subsidence to be up to 2 cm yr<sup>-1</sup> during 2015–2018, using InSAR pairs that spanned the same seasonal interval but in different years. The magnitude of subsidence and the spatial patterns are qualitatively reasonable as thermokarst subsidence compared to observations using field surveys and high-resolution optical images. L-band InSAR was effective in maintaining coherence over a long period for a partially forested thermokarst-affected area, which resulted in deriving the inter-annual subsidence by the stacking using four interferograms. The advantage of the persistent coherence in L-band InSAR is crucial to better understand thermokarst processes in permafrost regions.

**Keywords:** Permafrost, Thermokarst, Central Yakutia, Siberia, InSAR, Stacking, L-band, ALOS, ALOS-2



Graphical abstract

\*Corresponding author: Takahiro Abe, [abe.takahiro2@jaxa.jp](mailto:abe.takahiro2@jaxa.jp)

# Seasonal and transient surface displacements in the Kumamoto area, Japan, associated with the 2016 Kumamoto earthquake: implications for seismic-induced groundwater level change

Kazuya Ishitsuka\*, Takeshi Tsuji, Weiren Lin, Makoto Kagabu and Jun Shimada

*Earth, Planets and Space* 2020, 72:144 DOI: 10.1186/s40623-020-01275-2

Received: 29 December 2019, Accepted: 17 September 2020, Published: 9 October 2020

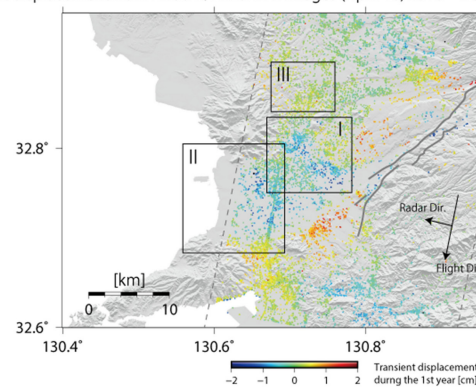


## Abstract

The 2016 Kumamoto earthquake sequence on April 14 ( $M_w$  6.2) and April 16 ( $M_w$  7.0) altered the regional groundwater level. To better understand the relationship between groundwater level change and surface displacement, we estimated surface displacement in the Kumamoto area (Japan) using persistent scatterer interferometry from 19 ALOS/PALSAR images acquired between January 7, 2007 and March 5, 2011, 28 ALOS-2/PALSAR-2 images acquired between April 17, 2016 and December 10, 2018, and 113 Sentinel-1 images acquired between May 26, 2016 and December 30, 2018. Our estimation shows that transient surface displacement occurred following the 2016 Kumamoto earthquake sequence, together with seasonal surface displacement that was not detected from the 2007–2011 images. We suggest that a portion of the transient displacement occurred via groundwater drawdown through new ruptures that formed owing to the 2016 Kumamoto earthquake sequence and sediment compaction. Seasonal surface displacements detected after the 2016 Kumamoto earthquake sequence are linked to groundwater level variations.

**Keywords:** Post-seismic displacement, Groundwater, Persistent scatterer interferometry, The 2016 Kumamoto earthquake sequence, PALSAR-2, PALSAR, Sentinel-1

Transient displacement from ALOS-2/PALSAR-2 images (April 18, 2016–December 10, 2018)



Graphical abstract

\*Corresponding author: Kazuya Ishitsuka, [ishitsuka.kazuya.4w@kyoto-u.ac.jp](mailto:ishitsuka.kazuya.4w@kyoto-u.ac.jp)

# Precursory ground deformation of the 2018 phreatic eruption on Iwo-Yama volcano, revealed by four-dimensional joint analysis of airborne and spaceborne InSAR

Shohei Narita\*, Taku Ozawa, Yosuke Aoki, Masanobu Shimada, Masato Furuya, Youichiro Takada and Makoto Murakami

*Earth, Planets and Space* 2020, 72:145 DOI: 10.1186/s40623-020-01280-5

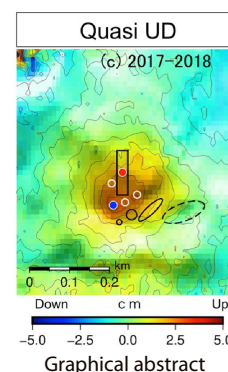
Received: 8 April 2020, Accepted: 23 September 2020, Published: 9 October 2020



## Abstract

We present detailed maps of local-scale 3D deformation preceding the 2018 phreatic eruption at Iwo-yama volcano (south of Kyushu Island, Japan), using a combination of airborne and spaceborne Interferometric Synthetic Aperture Radar (InSAR) data. The 3D and 2.5D deformation maps obtained at different periods allow us to successfully track their spatiotemporal evolution and to infer the transition of subsurface conditions responsible for the precursory deformation observed from 2014 to 2018. From 2014 to 2016, ground inflation depicted an axisymmetric pattern with the maximum displacement at the center of the deformed area. However, from 2016 to 2018, an inflation peak moved to the southern edge of the area deformed during 2014–2016 and became more localized, which was close to the newly generated vents in the 2018 eruption. Modeling of the inflations suggests that pressurization within a crack at a depth of 150 m beneath the Iwo-yama geothermal area caused the 2014–2016 deformation and had continued until the 2018 eruption. Modeling results highlight the persistence of the local ground inflation pattern just above the southern edge of the crack, which suggests the presence of a shallower inflation source contributing to the local inflation. Consequently, we interpret the sequence of these deformations as follows: from 2014, deeper-rooted fluid started to inject into a fluid-saturated crack at 150-m depth, which caused the 2014–2016 deformation. Then, after 2016, the crack inflation continued because of the continuous fluid injection and formed another pressurized part directly above the southern tip of the crack. Additionally, the results of the time-series analysis of the satellite InSAR data revealed that the local inflation started around April 2017 for which thermal activity including a mud emission became pronounced around the location of the local inflation. As a result of an episodic increase in supply rate of magmatic fluids from a deep magma reservoir from early 2018, a phreatic eruption finally occurred in the vicinity of the most deformed point, providing a clue for predicting future eruption sites, as was also observed in the Hakone 2015 eruption.

**Keywords:** InSAR, Phreatic eruption, Ground inflation, Volcanic hydrothermal system, Airborne SAR, Iwo-yama



\*Corresponding author: Shohei Narita, narita.shohei.6n@kyoto-u.ac.jp

# Postseismic deformation following the 2016 Kumamoto earthquake detected by ALOS-2/PALSAR-2

Manabu Hashimoto

*Earth, Planets and Space* 2020, 72:154 DOI: 10.1186/s40623-020-01285-0

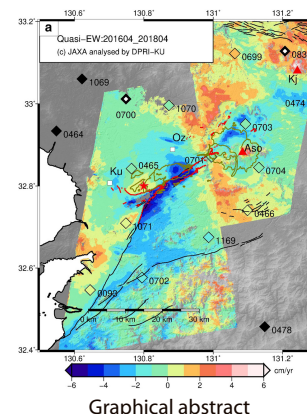
Received: 31 March 2020, Accepted: 30 September 2020, Published: 20 October 2020



## Abstract

I have been conducting a study of postseismic deformation following the 2016 Kumamoto earthquake using ALOS-2/PALSAR-2 acquired till 2018. I apply ionospheric correction to interferograms of ALOS-2/PALSAR-2. L-band SAR gives us high coherence enough to reveal surface deformation even in vegetated or mountainous area for pairs of images acquired more than 2 years. Postseismic deformation following the Kumamoto earthquake exceeds 10 cm during 2 years at some spots in and around Kumamoto city and Aso caldera. Westward motion of ~6 cm/year was dominant on the southeast side of the Hinagu fault, while westward shift was detected on both sides of the Futagawa fault. The area of latter deformation seems to have correlation with distribution of pyroclastic flow deposits. Significant uplift was found around the eastern Futagawa fault and on the southwestern flank of Aso caldera, whose rate reaches 4 cm/year. There are sharp changes across several coseismic surface ruptures such as Futagawa, Hinagu, and Idenokuchi faults. Rapid subsidence between Futagawa and Idenokuchi faults also found. It is confirmed that local subsidence continued along the Suizenji fault, which newly appeared during the mainshock in Kumamoto City. Subsidence with westward shift of up to 4 cm/year was also found in Aso caldera. Time constant of postseismic decay ranges from 1 month to 600 days at selected points, but that postseismic deformation during the first epochs or two is dominant at point in the Kumamoto Plain. This result suggests multiple source of deformation. Westward motion around the Hinagu fault may be explained with right lateral afterslip on the shallow part of this fault. Subsidence along the Suizenji fault can be attributed to normal faulting on dipping westward. Deformation around the Hinagu and Idenokuchi faults cannot be explained with right lateral afterslip of Futagawa fault, which requires other sources. Deformation in northern part of Aso caldera might be the result of right lateral afterslip on a possible buried fault.

**Keywords:** Kumamoto earthquake, Postseismic deformation, ALOS-2/PALSAR-2, Ionospheric correction, InSAR



Corresponding author: Manabu Hashimoto, hashimoto.manabu.7e@kyoto-u.ac.jp

# Surface deformation evolution in the Pearl River Delta between 2006 and 2011 derived from the ALOS1/PALSAR images

Genger Li, Guangcai Feng\*, Zhiqiang Xiong, Qi Liu, Rongan Xie, Xiaoling Zhu, Shuran Luo and Yanan Du

*Earth, Planets and Space* 2020, **72**:179 DOI: 10.1186/s40623-020-01310-2

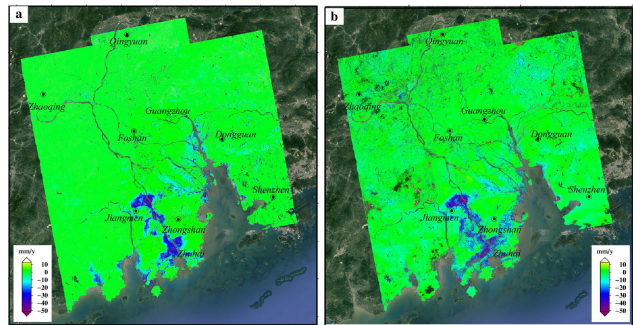
Received: 27 May 2020, Accepted: 9 November 2020, Published: 26 November 2020



## Abstract

This study monitors the land subsidence of the whole Pearl River Delta (PRD) (area:  $\sim 40,000 \text{ km}^2$ ) in China using the ALOS1/PALSAR data (2006–2011) through the SBAS-InSAR method. We also analyze the relationship between the subsidence and the coastline change, river distribution, geological structure as well as the local terrain. The results show that (1) the land subsidence with the average velocity of 50 mm/year occurred in the low elevation area in the front part of the delta and the coastal area, and the area of the regions subsiding faster than 30 mm/year between 2006 and 2011 is larger than  $122 \text{ km}^2$ ; (2) the subsidence order and area estimated in this study are both much larger than that measured in previous studies; (3) the areas along rivers suffered from surface subsidence, due to the thick soft soil layer and frequent human interference; (4) the geological evolution is the intrinsic factor of the surface subsidence in the PRD, but human interference (reclamation, ground water extraction and urban construction) extends the subsiding area and increases the subsiding rate.

**Keywords:** Pearl river delta, Natural evolution, Surface subsidence, SBAS-InSAR



Graphical abstract

\*Corresponding author: Guangcai Feng, fredgps@qq.com

# Information for Contributors

## *General*

1. Manuscripts should be submitted through the journal's Editorial Manager system (<https://www.editorialmanager.com/epsp/default.aspx>).
2. Only papers not previously published will be accepted, and the emphasis is on the originality of concept or observation.
3. Five varieties of article types are available.
  - 3.1 "Full Paper" without word limit.
  - 3.2 "Express Letter" has a limit of 5000 words including the main text, figure legends and table legends. The sum of the number of figures and tables should be less than or equal to 5.
  - 3.3 "Frontier Letter" can be submitted upon invitation by the Editor-in-Chief.
  - 3.4 "Technical Report" describes the technical development of instrument or software.
  - 3.5 "Comment" is a substantial re-analysis of a previously published article in the journal. "Comment" should not exceed 1000 words.
4. Authors retain the copyright, and distribution of articles is free under the CC BY license.

## *Technical*

1. Manuscripts should be written in English with double spacing.
2. Each manuscript should be organized in the following order: title, authors' names, affiliations, abstract, key words, main text, acknowledgement, appendix, references, and supplementary materials. A graphical abstract image must be uploaded during submission which should provide the reader with a visual description of the topic covered in the article.
3. The corresponding author should be clearly indicated.
4. The abstract is limited to 350 words and should be informative and include principal findings and conclusions. Please avoid abbreviations.
5. The main text can have multiple free headings.
6. High-resolution figures should be provided in the following format; PDF (preferred format for diagrams), PNG (preferred format for photos or images), EPS, TIFF, JPEG, BMP. The graphical abstract should be approximately 920 × 300 pixels and should be uploaded as a JPEG, PNG or SVG file.
7. References must follow the Springer Basic style.

## *Correspondence*

If you have any questions, please contact [info@springeropen.com](mailto:info@springeropen.com).

---

© EPS Steering Committee 2022 All rights reserved.

A Grant-in-Aid for Publication of Scientific Research Results (19HP1001) from Japan Society for the Promotion of Science is used for printing.

# Contents

L-band Synthetic Aperture Radar: Current and future applications to Earth sciences ..... Yosuke Aoki, Masato Furuya, Francesco De Zan, Marie-Pierre Doin, Michael Eineder, Masato Ohki and Tim J. Wright	1
Detection of triggered shallow slips caused by large earthquakes using L-band SAR interferometry ..... Satoshi Fujiwara, Takayuki Nakano and Yu Morishita	5
Surface creep rate distribution along the Philippine fault, Leyte Island, and possible repeating of $M_w \sim 6.5$ earthquakes on an isolated locked patch .....Yo Fukushima, Manabu Hashimoto, Masatoshi Miyazawa, Naoki Uchida and Taka'aki Taira	5
Surface deformation of Asama volcano, Japan, detected by time series InSAR combining persistent and distributed scatterers, 2014–2018 .....Xiaowen Wang, Yosuke Aoki and Jie Chen	6
Determination of the dipping direction of a blind reverse fault from InSAR: case study on the 2017 Sefid Sang earthquake, northeastern Iran .....Nematollah Ghayournajarkar and Yo Fukushima	6
Landslide detection in mountainous forest areas using polarimetry and interferometric coherence ..... Masato Ohki, Takahiro Abe, Takeo Tadono and Masanobu Shimada	7
Spatiotemporal behavior of a large-scale landslide at Mt. Onnebetsu-dake, Japan, detected by three L-band SAR satellites ..... Youichiro Takada and George Motono	7
Surface displacement revealed by L-band InSAR analysis in the Mayya area, Central Yakutia, underlain by continuous permafrost.....Takahiro Abe, Go Iwahana, Petr V. Efremov, Alexey R. Desyatkin, Takumi Kawamura, Alexander Fedorov, Yuri Zhegusov, Kazuki Yanagiya and Takeo Tadono	8
Seasonal and transient surface displacements in the Kumamoto area, Japan, associated with the 2016 Kumamoto earthquake: implications for seismic-induced groundwater level change ..... Kazuya Ishitsuka, Takeshi Tsuji, Weiren Lin, Makoto Kagabu and Jun Shimada	8
Precursory ground deformation of the 2018 phreatic eruption on Iwo-Yama volcano, revealed by four-dimensional joint analysis of airborne and spaceborne InSAR .....Shohei Narita, Taku Ozawa, Yosuke Aoki, Masanobu Shimada, Masato Furuya, Youichiro Takada and Makoto Murakami	9
Postseismic deformation following the 2016 Kumamoto earthquake detected by ALOS-2/PALSAR-2 ..... Manabu Hashimoto	9
Surface deformation evolution in the Pearl River Delta between 2006 and 2011 derived from the ALOS1/PALSAR images ..... Genger Li, Guangcai Feng, Zhiqiang Xiong, Qi Liu, Rongan Xie, Xiaoling Zhu, Shuran Luo and Yanan Du	10